VTT Technical Research Centre of Finland

Two-stage SQUID amplifier for the frequency multiplexed readout of the X-IFU x-ray camera

Kiviranta, Mikko; Grönberg, Leif; Puranen, Tuomas; Van der Kuur, Jan; Beev, Nikolai; Salonen, Jaakko; Hazra, Dibyendu; Korpela, Seppo

[Link to publication]

Two-stage SQUID amplifier for the frequency multiplexed readout of the X-IFU X-ray camera

Mikko Kiviranta, Leif Grönberg, Tuomas Puranen, Jan van der Kuur, Nikolai Beev, Jaakko Salonen, Dibyendu Hazra and Seppo Korpela

Abstract—The X-ray Integral Field Unit (X-IFU) is a cryogenic X-ray camera intended for the ATHENA space observatory. Its focal plane will contain a kilopixel array of Transition Edge Sensors (TESs), originally intended to be read out by a Frequency Domain Multiplexer involving 40 carrier frequencies in the 1 - 5 MHz range per readout channel. We review dimensioning principles and fabrication of a SQUID tandem, operating at 50 mK and 2 K temperatures, intended to amplify the multiplexed signal from the TES array. The first measurements indicate a 40 h coupled energy resolution in the relevant frequency band, and sufficient linearity to reach the required 1% total harmonic distortion. Additionally, we describe the non-multiplexed amplifier SQUID for the X-IFU anti-coincidence detector.

Index Terms— SQUID designs and applications, Josephson device fabrication, Transition-edge sensors (TES) devices, Multiplexing

I. INTRODUCTION

THE X-ray Integral Field Unit (X-IFU) [1] is a is a cryogenic X-ray camera to be carried onboard the Advanced Telescope for High Energy Astrophysics (ATHENA) [2], a (L)arge-class mission by the European Space Agency (ESA). The X-IFU will contain an array of 3 168 Transition Edge Sensor (TES) calorimeters [3] with Frequency Domain Multiplexing (FDM) [4] as the original baseline TES readout technique. The TES array is under development at NASA / Goddard Space Flight Center (GSFC).

Similarly, the SPICA Far Infrared Instrument (SAFARI) was the planned sub-mm wave camera to be carried onboard the Space Infrared Telescope for Cosmology and Astrophysics (SPICA) [5], a candidate for the fifth launch opportunity for a (M)edium-class mission in the ESA Cosmic Vision programme. The SAFARI was planned to contain order-of 3 500 TES bolometers with FDM readout [6]. The SPICA mission was however discontinued a few weeks before submission of this paper. An example of a ground-based FDM detector system is [7].

Fig. 1. Simplified diagram of the SQUID tandem consisting of the single front end SQUID at T = 50 mK, the 4-parallel 40-series SQUID array (booster) at T = 2 K and the LNA at room temperature. The dc-coupled LNA utilizes a differential pair of 2 x 3 paralleled NESG3031 discrete SiGe transistors to reach u_N = 0.5 nV/Hz$^{1/2}$ voltage and i_N = 2 pA/Hz$^{1/2}$ current noise, with 180 V/V gain (45 V/V from the differential pair, 4 V/V from the buffer) and Δf > 40 MHz bandwidth. Feedback through the R_{TR} resistors can be activated via photoMOS switches to create a $|Z_{IN}| \approx 150\ \Omega$ virtual LNA input resistance whose noise temperature is less than the ambient [11]. The booster includes a voltage-sampling local feedback circuit [12], which can be optionally activated by wire bonding.

Motivated by the X-IFU and SAFARI instruments, the VTT-SRON collaboration has been developing a SQUID-based FDM readout chain for many years, the most recent development being the switch from pillar-type [8] Josephson junctions (JJs) to crossed-line SWAPS [9] JJs. Roughly the same time as the first design iteration of the SWAPS-based SQUIDs for X-IFU was finished and testing underway in February 2020, the X-IFU consortium chose Time Domain Multiplexing (TDM) [10] as the baseline readout technique, putting further FDM development on the hold. We review here the status of the SQUID development after the first SWAPS design iteration and the laboratory tests at VTT and SRON.

Fig. 2. Fabrication steps to form a SWAPS Josephson junction [9]. From left to right: The lower stripe is patterned from Nb-Al/AlOx-Nb trilayer. Sloped side-wall spac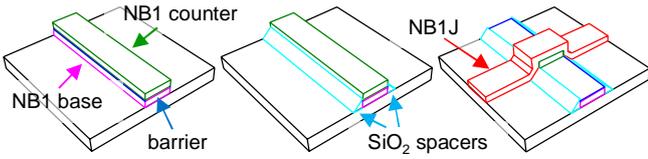ers [26] are deposited. The crossing Nb stripe is deposited and patterned. The Josephson junction is formed at the overlap of the two stripes.

II. THE SQUID TANDEM

The SQUID tandem for X-IFU (Fig. 1) refers to two cascaded SQUID amplification stages, the front-end (FE) SQUID and booster (AMP) SQUID, followed by a room temperature Low Noise Amplifier (LNA) and a digitizer. Digitization in the VTT setup is performed by the Red Pitaya [13] acquisition unit. The tandem shown here is an upgrade of [14] and [15], and it attempts to use a smaller number of more 'muscular' SQUID cells in the arrays, heuristically in order to reduce the number of degrees of freedom which may de-cohere.

In FDM the TES currents are combined via LC resonators into a summing node (see eg. Fig. 1 of [6]), and the sum of currents drive the FE input coil (Fig. 1). In FDM the FE input should present an ideal ammeter, i.e. its impedance should be an ideal short, to avoid pixel-to-pixel crosstalk and reduced total bandwidth [16]. In practice the FE input inductance should be extremely low $L_{IN,FE} \approx 1$ nH, which leads to two difficulties: 1) energy resolution requirement of the FE SQUID $\varepsilon = \frac{1}{2}L_{IN}i_n^2$ becomes challenging when the input current noise i_n is constrained; and 2) parasitic inductance of interconnects may be significant. The former can be alleviated via a power combiner more complex than the simple T-junction [17]. The FE SQUID reviewed here, the type 'M1', is the X-IFU baseline version implementing the simple T-junction combiner and having a low $L_{IN,FE}$.

The purpose of the two SQUID stages is to raise the signal power created by an maximal-energy x-ray event from the level at the TES output $P_{O,TES} \approx 1$ pW (-87 dBm) to the level $P_{I,LNA} \approx 20$ nW (-47 dBm) at the LNA input, sufficiently high above the LNA noise floor to cover the planned dynamic range. Operated as a class-A amplifier, the FE SQUID dissipates $P_{D,FE} \approx 1$ nW to generate the available signal power of $P_{O,FE} \approx 100$ pW (-70 dBm) and the booster SQUID dissipates $P_{D,AMP} \approx 200$ nW to generate $P_{O,AMP} \approx 20$ nW. Even if the class-B operation [18], [19] could improve the power efficiency P_O/P_D, the dissipation forces one to locate the booster SQUID at the $T = 2$ K stage of the X-IFU refrigerating chain. The FE SQUID resides at the $T = 50$ mK stage close to the TES detectors.

The X-IFU FDM was designed to use 40 carrier frequencies with $\Delta f = 100$ kHz in the 1…5 MHz band. The two dominant bandwidth limits of the tandem are the L/R cutoff in the interstage wiring between the FE and AMP SQUID, and the RC cutoff in the AMP - LNA wiring. The $L = L_{ISTG} + L_{IN,AMP}$ in the L/R includes the 50 mK - 2 K wiring inductance L_{ISTG} and the input inductance of the booster $L_{IN,AMP}$, while we want to keep

TABLE I: MASK LAYERS IN FABRICATION

Mask layer name	Material, thickness	Comments
NB1	Nb 150 nm, Al 10 nm, AlOx, Nb 100 nm	Lower SWAPS stripe for JJs, with spacers [9].
NB1J	Nb 120 nm	Crossing SWAPS stripe.
RES	TiW 90 nm	Target 5 Ω / square.
INS1[a]	SiO₂ 100 + 100 nm	100 nm under RES, 100 nm on top.
NB2[b]	Nb 200 nm	Second wiring layer.
INS2[a]	SiO₂	CMP planarized, thickness varies.
NB3	Nb 200 nm	Third wiring layer.
PASS[a]	SiO₂ 250 nm	Passivation.
AU	Au 250 nm	Deep contact windows to RES, Au lift-off patterned.

[a] All SiO₂ layers are PECVD deposited at 180 °C.
[b] BREAKBEN fabrication process [23] followed up to here

$L_{ISTG} \leq L_{IN,AMP}$ to avoid signal loss in the inductive divider formed by the two. The resistance R in the L/R cutoff is the dynamic output resistance of the FE SQUID, which we attempted to raise as high as power dissipation budget allows, reaching nominally $R_{D,FE} \approx 12.5$ Ω.

The RC cutoff could be alleviated by lowering the dynamic resistance of the booster $R_{D,AMP}$. The C here is the parasitic capacitance of the 2 K - 300 K wiring. We have chosen to combine a moderate $R_{D,AMP} \approx 125$ Ω, nominally, with terminating the 2 K - 300 K wiring resistively at LNA and making the wiring behave more like a transmission line. The terminating resistor is virtual, generated by a feedback technique in the LNA (Fig. 1) to make its noise temperature less than the ambient temperature [11]. The virtual suppression of the SQUID gain $dV/d\Phi$ due to the LNA loading does not affect the signal-to-noise ratio (SNR); it is feasible to reduce $|Z_{IN}|$ of the LNA even to zero (i.e. make it a transimpedance amplifier, as with voltage-biased SQUIDs [20]) and still have the SNR determined as the ratio of the *unsuppressed* $dV/d\Phi$ of the booster and the voltage noise u_N of the LNA. The LNA is a 2012 upgrade of our previous version [14] and intended for laboratory work only. The X-IFU flight LNA is under development in the University of Paris [21].

III. SQUID FABRICATION

The SQUIDs are fabricated in the Micronova clean room [22] on 150 mm Si wafers, using projection lithography with the Canon FPA3000-i4 projection stepper. The clean room update to use 200 mm wafers in all processes is underway.

The fabrication process is an upgrade of the one used in the BREAKBEN project [23], with the third Nb superconductive wiring layer and gold layer for cooling fins [24] added. The SiO₂ insulator below the third wiring is Chemically-Mechanically (CMP) polished, facilitating additional wiring layers for eg. RSFQ implementation [25] in future. The list of mask layers is shown in the Table 1.

Josephson junctions fabricated with $J_C = 1.5$ kA/cm² critical current density are located in the lowermost layer, using the SWAPS [9] process outlined in Fig. 2. Their shunt resistors are
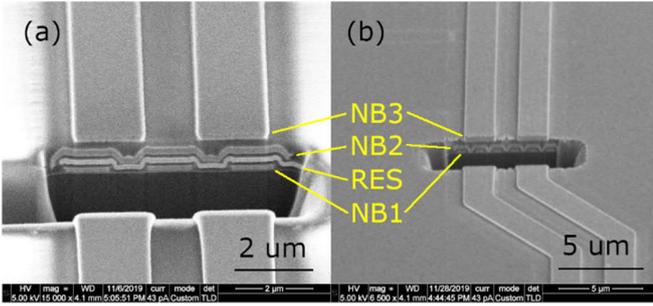
Fig. 3. (a) Cross-section of the metal/insulator stack present in the standard SQUID cell, produced by Focussed Ion Beam (FIB) etching: see Fig. 4 for the location of the cut. The lowermost niobium wiring layer NB1 contains a 3-turn input coil at 1 μm linewidth and 1 μm insulation gap. The resistive layer above it contains capacitively coupled intracoil resistors [28] in some device variants. The next NB2 wiring layer contains the 6 μm wide SQUID loop, and the top NB3 wiring layer contains two one-turn coils for flux setpoint and local feedback. (b) A device variant with 6-turn input coil using 0.5 μm / 0.5 μm design rule. The observed degraded magnetic coupling from the midmost turns discourages the use of as dense input coil as this.

Fig. 4 (Left) SEM microphotograph of the SQUID region of the 2×2 mm Front End chip. The top wiring layer (NB3) is visible while CMP obscures lower layer visibility. The region contains the $L_{SQ} = 70$ pH gradiometric SQUID loop and the $L_{DEC} = 35$ pH decoupling transformer. The FIB cut used to produce the Fig 3 cross-section is visible in the left sub-loop of the gradiometer. (Right) Schematic of the Front End chip shows the SQUID, the input-feedback decoupler, a balanced port for the Baseband Feedback [30], a setpoint coil, and multiple inputs driving the FDM summing node. Inputs are equipped with 0.5 nH / 0.5 Ω and SQUID outputs with 15 nH / 10 Ω L/R-filters.

patterned out of titanium-tungsten film for good millikelvin performance [27]. The niobium layers NB1, NB2 and NB3 are patterned with $Cl_2 + CF_4$ plasma and the INS1 and INS2 contact windows in the SiO_2 insulator layers with CHF_3 plasma. The Au is deposited on a deep via to reach the TiW layer and patterned with lift-off. An example cross section of the realized film stack is shown in Fig. 3. The 1 μm linewidth / 1 μm gap design rule for Nb layers has been followed in the X-IFU devices, although the process is capable to implement 0.5 μm / 0.5 μm design rule reliably (Fig. 3b). The INS1 contact windows are 1×1 μm in SQUID designs, but 0.6×0.6 μm windows can be opened reliably. Due to uncertainty of the final insulator material and etch method during process development, the INS2 contact windows were drafted as 3.2 μm in the masks, but 0.6×0.6 μm can be opened reliably with plasma in the CMP SiO_2.

IV. SQUID DIMENSIONING

A. Front end SQUID

The basic building block is a cascadeable SQUID cell with gradiometric main loop of $L_{SQ} = 70$ pH inductance. Widths of all niobium structures are $w \leq 6$ μm to avoid flux trap formation in the Earth's field [29], whereby both front-end and booster devices can be operated without superconducting or mu-metal shields[1]. The cell is equipped with 0.8×0.8 μm JJs whose nominal critical current is $I_C = 9.6$ μA, and with $R_S = 17.5$ Ω shunt resistors. The cell bias feed can be arranged symmetrically or asymmetrically. The nominal cell dissipation is $P_D \approx 1$ nW. The cells are furnished with 3-turn input coils, yielding $M^{-1} \approx 14$ μA/Φ_0 periodicity.

---

[1] Magnetic shielding is foreseen in the X-IFU focal plane assembly for protection against electromagnetic interference pickup, even if the SQUIDs are flux trap resistant.
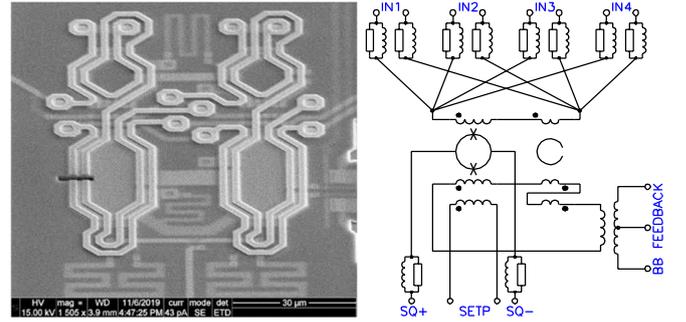
Internal schematic of the front-end SQUID is shown in the Fig. 4. An asymmetrically biased version 'M1' was intended for the X-IFU. It was to be operated on the shallow slope of the flux response in order to reach the FDM requirement of 1% total harmonic distortion (THD) at the nominal ac flux excitation. The SQUID is equipped with a decoupling transformer to reduce the interaction of the baseband feedback (BBFB) [30] with the TES detectors. We have measured $L_{IN,FE} \approx 1.1$ nH input inductance at the summing node.

B. Booster SQUID

The booster SQUID is a 40-series 4-parallel array of symmetrically biased SQUID cells on a 4×4 mm chip, designated as the type 'N2'. Not shown in the simplified schematic (Fig. 1), there is a middle tap available both in the SQUID series array output and the input coil, facilitating both balanced and single-ended circuit configurations. The booster is equipped with a coil for local negative feedback, to create asymmetric flux response (Fig. 5b) with a shallow slope, on which the FDM requirement of 1% THD is reached. The chosen feedback condiguration is voltage-sampling (V-FB) [11], because negative V-FB tends to simultaneously lower the $R_{D,AMP}$, an advantage for the tandem operation. When the V-FB is activated, loading by the 2×210 Ω on-chip voltage-sampling resistors suppress the modulation depth somewhat, as seen in the difference between Fig. 5 (a) and (b). The suppressing effect is in line with the original device dimensioning.

C. CryoAC readout

In addition to the main TES array, there is a non-multiplexed 4-pixel anti co-incidence TES detector [31] in the X-IFU focal plane array. Non-multiplexed readout of these TESs involves single stage SQUID amplifiers, fabricated in the same process
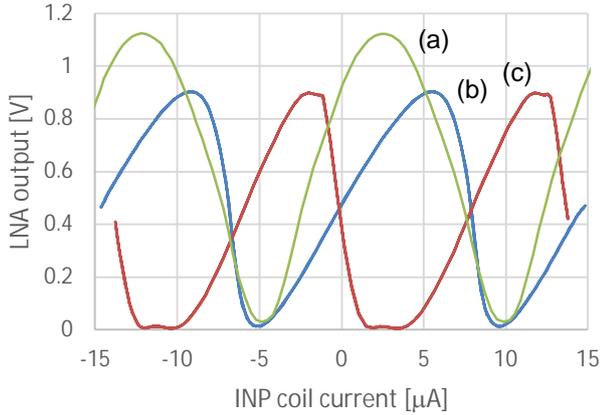
Fig. 5. Flux response of a booster SQUID when the local feedback is (a) inactive and (b) active. The trace (c) shows flux response of the FE SQUID measured through the shallow slope of the booster SQUID while the local feedback is active; the slight foldback at the sweep extrema indicates that the FE current swing is slightly too large to fit within the monotonous range of the booster. The LNA virtual termination is off in all cases. The booster SQUID voltage for traces (a) and (b) is obtained by dividing the LNA output voltage by 180. The front-end SQUID output current scale can not be deduced as easily from the trace (c) since the transresistance through the booster is not constant.
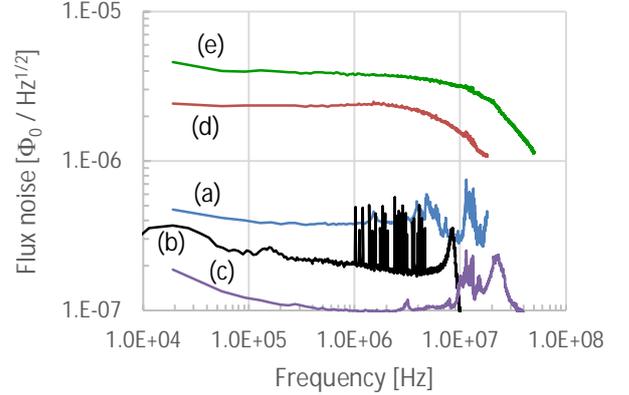

Fig. 6. (a), (b), (c): Some flux noise spectra: (a) FE SQUID at $T = 4.2$ K recorded through the booster SQUID, local feedback active, both SQUIDs on their shallow slopes. (b) FE SQUID at $T = 20$ mK recorded through the booster SQUID in the SRON setup. The spikes in the spectrum are due to 24 LC resonators connected to the FE SQUID input. (c) The booster SQUID alone at $T = 4.2$ K on shallow slope with local feedback.
(d), (e): Frequency responses obtained with white pseudorandom noise flux excitation of the tandem (corresponding noise a) and plain booster (corresponding noise c).

wafers as the FE and booster SQUIDs. The CryoAC amplifiers, designated as the type 'M4', are 2-series SQUID arrays, whose constituent SQUIDs are a variant of the standard SQUID cell. The $L_{SQ} = 70$ pH main loop and the 3-turn input coil are similar, but Josephson junctions are 0.6×0.6 μm with the nominal critical current $I_C = 5.4$ μA, equipped with $R_S = 33$ Ω shunt resistors. The 'M4' SQUID includes on-chip 0.5 mΩ and 2.5 mΩ resistors for TES biasing.

The target of the configuration is to obtain high enough gain $dV/d\Phi$ within the $P_D \approx 1$ nW dissipation budget, so that sufficiently low flux noise can be obtained from a single SQUID stage. We have observed $dV/d\Phi = 1$ mV/Φ_0 gain and $\Phi_N < 1$ μΦ_0/Hz$^{1/2}$ in these devices when using our SiGe LNA for readout.

V. RESULTS AND DISCUSSION

Flux-to-voltage response of the 'N2' booster at $T = 4.2$ K is shown in Fig. 5 (a), exhibiting $\Delta V \approx 6$ mV modulation depth. When the wire bonds for the voltage-sampling feedback coil are attached, the trace (b) of Fig. 5 is obtained. In the traces the virtual termination of the LNA is inactive. When the termination is activated, the modulation depth ΔV is suppressed; although this does not affect the LNA-dominated SNR, it affects the loop gain of the local feedback and makes the shallow slope less linear. It turns out, however, that sufficient booster-to-LNA bandwidth can be obtained without the termination, so that close to X-IFU compliant linearity and THD is reached concurrently with the bandwidth. The choice of terminated vs. unterminated LNAs in the X-IFU system is still open.

The Fig. 5 (c) shows the flux response of the complete tandem, i.e. FE SQUID current amplified by the booster SQUID.

The FE steep and shallow slopes are generated by the asymmetric bias feed. Asymmetric bias feed is equivalent to current-sampling feedback [12], beneficially increasing the dynamic resistance $R_{D,FE}$ on the shallow slope.

Frequency response of the tandem is the trace (d) in Fig. 6, indicating -3 dB bandwidth of $\Delta f = 9$ MHz. The flux noise Fig. 6 (a) is measured at VTT in LHe, but the T = 50 mK flux noise in Fig. 6 (b) has been measured at SRON as a part of an FDM resonator test because the dilution refrigerator setup at VTT is presently suffering from EMI pickup. The $\Phi_N \approx 0.2$ μΦ_0/Hz$^{1/2}$ was reached. The SRON uses a single-ended ac-coupled LNA different from the LNA in Fig. 1. In traces (a) and (d) VTT LNA has been used, with the virtual termination inactive.

To verify functioning of the VTT LNA with the termination active, we have measured -3 dB bandwidth $\Delta f = 21$ MHz.(Fig. 6e) and flux noise $\Phi_N \approx 0.1$ μΦ_0/Hz (Fig. 6c) for the booster SQUID, with the FE SQUID disconnected.

VI. CONCLUSION

We observe the SQUID tandem performance close to or within the FDM requirements for the X-IFU instrument. Although the FDM development is discontinued, we foresee the booster SQUID can be used as a part of the new TDM system for X-IFU [10] without significant modifications. The CryoAC readout SQUID is also close to or within the requirements. The radiation hardness test campaign is expected in the spring 2021. These devices are a good starting point for the next design iteration, likely to provide SQUIDs for the demonstration model of the X-IFU instrument.

REFERENCES

[1] F. Pajot et al., "The Athena X-ray integral field unit (X-IFU)," *J. Low Temp. Phys* ., vol. 193, pp. 901-907, 2018. Doi:10.1007/s10909-018-1904-5.

[2] [Online.] Available: https://sci.esa.int/web/athena.

[3] J. N. Ullom and D. A. Bennett, "Review of superconducting transition-edge sensors for X-ray and gamma-ray spectroscopy," *SuST*, vol. 28, 084003, 2015. Doi: 10.1088/0953-2048/28/8/084003.

[4] H. Akamatsu et al., "Progress in the development of frequency-domain multiplexing for the X-ray Integral Field Unit on board the Athena mission," *J. Low. Temp. Phys.*, vol. 199, pp. 737-744, 2020. Doi: 10.1007/s10909-020-02351-3.

[5] P. R. Roelfsema et al., "SPICA - a large cryogenic infrared space telescope Unveiling the obscured Universe", *arXiv:*1803.10438, 2018.

[6] R. A. Hijmering et al., "Readout of a 176 pixel FDM system for SAFARI TES arrays", *Proc. SPIE*, vol. 9914, 99141C-11, 2016. Doi: 10.1117/12.2231714.

[7] M. A. Dobbs et al., "Frequency multiplexed superconducting quantum interference device readout of large bolometer arrays for cosmic microwave background measurements," *Rev. Sci. Instr.,* vol. 83, 073113, July 2012. Doi: 10.1063/1.4737629 .

[8] M. Kiviranta et al., "Multilayer fabrication process for Josephson junction circuits cross-compatible over two foundries," *IEEE. Tran. Appl. Supercond.*, vol. 26, no. 6, 1100905, Sept. 2016. Doi: 10.1109/TASC.2016.2544821.

[9] L. Grönberg et al., "Side-wall spacer passivated sub-µm Josephson junction fabrication process," *SuST*, vol. 30, 125016, 2017. Doi: /10.1088/1361-6668/aa9411.

[10] M. Durkin et al., "Demonstration of Athena X-IFU compatible 40-row time-division-multiplexed readout", *IEEE Tran. Appl. Supercond.,* vol. 29, no. 5, 2101005, Aug. 2019. Doi: 10.1109/TASC.2019.2904472.

[11] W. S. Percival, "An electrically 'cold' resistance," *Wireless Engineer*, vol. 16, pp. 237-240, May 1939.

[12] M. Kiviranta, "SQUID linearization by current-sampling feedback," *SuST*, vol. 21, 045009, 2008. Doi: 10.1088/0953-2048/21/4/045009.

[13] [Online.] Available: https://redpitaya.readthedocs.io.

[14] M. Kiviranta, L. Grönberg and H.Sipola, "Two-stage locally linearized SQUID readout for frequency domain multiplexed calorimeter arrays," *SuST*, vol. 24, 045003, 2011. Doi: 10.1088/0953-2048/24/4/045003.

[15] L. Gottardi, M. Kiviranta, J. van der Kuur, H. Akamatsu, M. P. Bruijn and R. den Hartog, "Nearly quantum limited two-stage SQUID amplifiers for the frequency domain multiplexing of TES based X-ray and infrared detectors," *IEEE Tran. Appl. Supercond.,* vol. 25, no. 3, 2100404, June 2015. Doi: 10.1109/TASC.2014.2369234.

[16] J. van der Kuur et al., " Optimising the multiplex factor of the frequency domain multiplexed readout of the TES-based microcalorimeter imaging array for the X-IFU instrument on the Athena x-ray observatory," *Proc. SPIE*, vol. 9905, 99055R, 2016. Doi: 10.1117/12.2232830.

[17] M. Kiviranta, L. Grönberg and J. van der Kuur, "Two SQUID amplifiers intended to alleviate the summing node inductance problem in multiplexed arrays of Transition Edge Sensors," *arXiv:* 1810.09122, 2018.

[18] M. Kiviranta, "Low-dissipating push-pull SQUID amplifier for TES detector readout," *arXiv:* 1810.04706, 2018.

[19] M. Kiviranta, "Class-B cable-driving SQUID amplifier," *arXiv:* 2011.11741, 2020.

[20] M. Kiviranta and H. Seppä, "DC-SQUID electronics based on the noise cancellation scheme," *IEEE Tran. Appl. Supercond.,* vol. 5, no. 2, pp. 2146 - 2148, June 1995. Doi: 10.1109/77.403007 .

[21] D. Prêle et al., "SiGe integrated circuit developments for SQUID/TES readout," *J. Low Temp. Phys.,* vol. 193, pp. 455-461, March 2018. Doi: 10.1007/s10909-018-1886-3.

[22] [Online.] Available: https://www.micronova.fi.

[23] J. Luomahaara, M. Kiviranta, L. Grönberg, K. C. J. Zevenhoven and P. Laine, " Unshielded SQUID sensors for ultra-low-field magnetic resonance imaging," *IEEE Tran. Appl. Supercond.*, vol. 28, no. 4, 1600204, June 2018. Doi: 10.1109/TASC.2018.2791022.

[24] F. C. Wellstood, C. Urbina and J. Clarke, "Hot electron effect in the DC SQUID," *IEEE Tran. Magn.*, vol. 25, no. 2, pp. 1001-1004, March 1989. Doi: 10.1109/20.92457.

[25] L. Grönberg, J. Hassel, P. Helistö and M. Ylilammi, " Fabrication process for RSFQ/qubit systems," *IEEE Tran. Appl. Supercond.*, vol. 17, no. 2, pp. 952-954, July 2007. Doi: 10.1109/TASC.2007.897721.

[26] H. Ronkainen, G. Drozdy and S. Franssila, "The use of disposable double spacer and self-aligned cobalt silicide for LDD MOSFET fabrication,"

[27] *IEEE Electr. Dev. Lett.*, vol. 12, no. 3, March 1991. Doi: 10.1109/55.75732.

[27] M. Kiviranta, L. Grönberg and J. Hassel, "A multiloop SQUID and a SQUID array With 1-µm and submicrometer input coils," *IEEE Tran. Appl. Supercond.* vol. 22, no. 4, 1600105, Aug. 2012. Doi: 10.1109/TASC.2012.2190286.

[28] M. E. Huber et al.,"DC SQUID series arrays with intracoil damping to reduce resonance distortions," *Applied Superconductivity*, vol. 5, nos. 7-12, pp. 425-429, 1997. Doi: 10.1016/S0964-1807(98)00065-9.

[29] G. Stan, S. B. Field and J. Martinis, "Critical field for complete vortex expulsion from narrow superconducting strips", *PRL*, vol. 92, 097003, March 2004. Doi: 10.1103/PhysRevLett.92.097003.

[30] R. den Hartog et al., "Frequency domain multiplexed readout of TES detector arrays with baseband feedback," *IEEE Tran. Appl. Supercond*, vol. 21, no. 3, pp. 289-293, June 2011. Doi: 10.1109/TASC.2010.2101998.

[31] M. D'Andrea et al., "The Demonstration model of the ATHENA X-IFU cryogenic AntiCoincidence detector," *J. Low Temp. Phys.*, vol. 199, pp. 65-72, 2020. Doi: 10.1007/s10909-019-02300-9.